Improved Solar Absorptance of WC/Co Solar Selective Absorbing Coating with Multimodal WC Particles

Xiaobo Wang [1], Taoyuan Ouyang [1], Xiaohua Duan [1], Chengzhu Ke [1], Xuemin Zhang [1], Jie Min [2], Aang Li [1], Weiyang Guo [1] and Xudong Cheng [1,*

[1] State Key Laboratory of Advanced Technology for Materials Synthesis and Progressing, Wuhan University of Technology, Wuhan 430070, China; wangxiaobo6@163.com (X.W.); ouyangty@whut.edu.cn (T.O.); dxhua1350top@163.com (X.D.); ke305631703@yahoo.com (C.K.); jizhulezxm@163.com (X.Z.); keweili@mail.nwpu.edu.cn (A.L.); lkw917@126.com (W.G.)
[2] Hubei Collaborative Innovation Center for High-Efficiency Utilization of Solar Energy, Wuhan 430070, China; whutminj@163.com
* Correspondence: xdcheng54@126.com; Tel.: +86-27-8765-1841

Abstract: One type of multimodal (comprised of nanometer and sub-micrometer WC particles) and two types of conventional (comprised of nanometer and sub-micrometer WC particles, respectively) WC/Co powders were deposited on AISI 304L stainless steel substrates by using high velocity oxygen fuel spraying. The use of multimodal WC particles was indicated to have a beneficial effect on the solar absorptance (α) of the WC/Co coatings. The α of the multimodal WC coating reached 0.87, which was much higher than what can be achieved by either fine (0.82) or coarse powders (0.80) alone. By microstructural analysis, the enhancement in solar absorptance of the multimodal WC/Co coating was ascribed to the layer of distributed WC particles. During the thermal spraying, the nanostructured WC particles underwent rapid melting for the large specific surface area while the aggregated powders were heated, but not necessarily melted. The molten nano-WC would fill the available pores between the softened and heated aggregates, providing a layered distribution of WC particles for the spray-deposited coating. In this condition, the light-trapping in the multimodal coating will be enhanced due to the efficient light reflection among the multimodal WC particles, which contributes to the enhancement of solar absorptance.

Keywords: solar selective absorbing coating; high velocity oxygen fuel; selective absorbing properties

1. Introduction

Metal-dielectric coatings that employ highly solar-absorbent and IR-transparent materials deposited onto highly IR-reflective metal substrates, such as Co/WC [1,2], Pt/Al$_2$O$_3$ [3], Mo/Si$_3$N$_4$ [4] and W/AlN [5], have been denoted to develop solar selective absorbing coatings for high temperature photo-thermal conversion applications due to their excellent absorptance (α) performance in the wavelength range of solar radiation (0.3~2.5 μm) and low thermal emittance (ε) in the infrared region (2.5~25 μm) [6]. The metal-dielectric selective coatings can offer a high degree of flexibility for tuning the absorption and scattering cutoff wavelengths by particle and matrix constituents, particle sizes and concentrations, coating thickness, etc. [2,7]. By materials selection, composition optimization and structure design, various kinds of coatings with absorptance better than 0.90 and emittance lower than 0.20 were successfully fabricated.

However, these high solar absorptivity, solar selective coatings either need high cost and vacuum processes, such as chemical vapor deposition and sputtering, or they will exhibit bad spectral selectivity

around 1~2 μm [2]. In addition, the optical properties of these coatings will start to degrade with the coupled effects of air and high temperature, due to oxidation or diffusion of the metal elements into the dielectric matrix, which thus restricts their applications for future concentrating solar power operation at high temperatures (≥700 °C) [2].

High velocity oxygen fuel spraying (HVOF) is well suited to fabricate coatings for photo-thermal conversion at high temperatures thanks to its apparent advantages, such as lower particle temperature, higher powder particle velocity and shorter residence time [8]. Moreover, the low flame temperature can preserve the desirable WC phase, which compromises the density of the coating and the bond strength to the substrate, resulting in preferred mechanical performance and thermal stability. It has been well established that the powder morphology, spray parameters and type of feedstock could have a significant effect on the microstructure of the coating [9] and, in turn, the solar selectivity. The thermal sprayed coatings based on WC are widely used as hard coatings [10–12] and solar selective absorbing coatings [1,13]. However, enhancements in WC/Co coatings fabricated by nano-WC/Co powders have remained elusive due to the decarburization occurring under thermal spraying conditions.

In order to reduce the decarburization of the WC/Co coatings, substantial efforts have been made to use agglomerates as feedstock powders [10,14,15], which can minimize the contracting time of the powders that go through the high-temperature cycles due to the increase of momentum, thus limiting the amount of decarburization. Meanwhile, the agglomerated feedstocks also can create large impact forces as particles arrive at the substrate surface and promote strong particle-substrate adhesion which, in turn, leads to the formation of dense coatings [16,17]. Furthermore, the coarse and fine WC particles response differently under the combustion flame, which would lead to the formation of special microstructures. Thus, we can anticipate that the solar spectral properties of the multimodal WC/Co solar selective absorbing coating may be improved by using agglomerated feedstocks. However, only the hardness and abrasive wear resistance, rather than the solar spectral properties of these multimodal WC/Co coatings, have yet been investigated.

In the present work, a class of multi-scaled WC/Co agglomerated particles consisting of a mixture of sub-micrometer and nanometer WC particles was sprayed by employing HVOF. The optical properties and structure of the multimodal coating as well as two conventional coatings were investigated. The deposition behavior of the sprayed multimodal WC/Co solar selective absorbing coating was also discussed.

2. Materials and Methods

2.1. Agglomerated Feedstock Preparation

Two kinds of WC/Co powders were used in the present work, namely single sized and multimodal mixtures of spherical particles with carbide grain size of sub-micrometer (99.5 wt %, 2 μm, Aladdin, Shanghai, China), nanometer (99.5 wt %, 0.7 μm, Aladdin, Shanghai, China), and sub-micrometer plus nanometer grains, as illustrated in Table 1. The spray powders with a size of approximately 45 μm, measured by laser granulometry (Bettersize, Dandong, China), were produced from the spray dry and conversion as shown in Figure 1a–f, of which, the feedstock powders exhibited agglomerated spherical morphology. It can be seen that the multimodal agglomerated feedstock shown in Figure 1c, fconsist of WC particles and Co phase.

Table 1. Compositions of the feedstock powders used in the HVOF (High velocity oxygen fuel spraying) spraying.

Sample Number	Composition, wt %
A1	80% Co + 20% sub-micrometer WC
A2	80% Co + 20% nanometer WC
A3	80% Co + 10% sub-micrometer WC + 10% nanometer WC

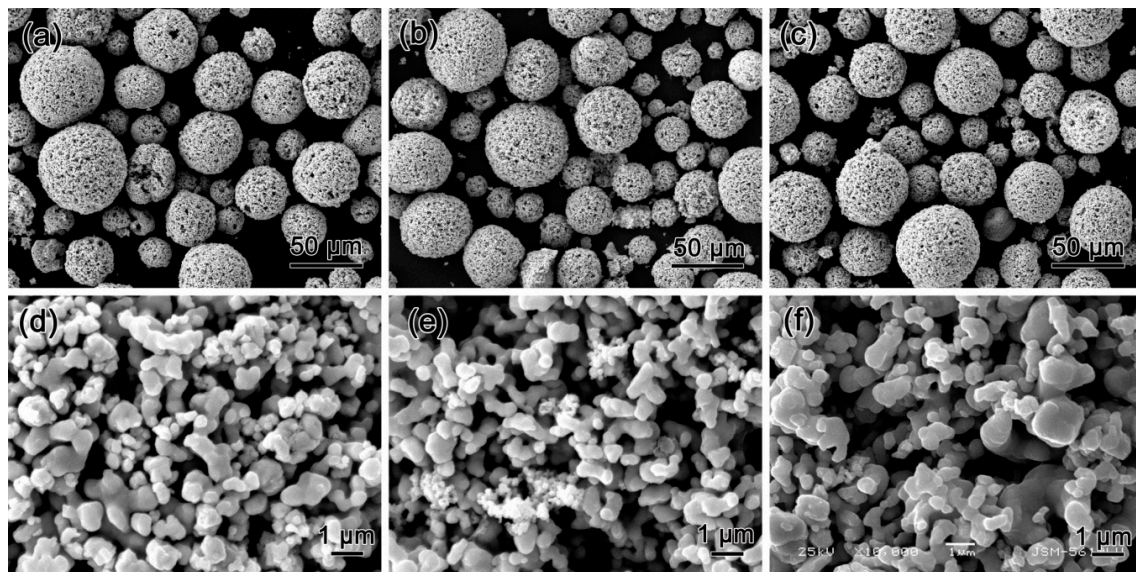**Figure 1.** SEM images of conventional and multimodal mixtures of the agglomerated spherical powders produced by spray dry and conversion: (**a**,**d**) sample A1; (**b**,**e**) sample A2; (**c**,**f**) sample A3.

2.2. Coating Preparation

AISI 304L stainless steel substrates (30 mm × 40 mm × 1 mm) were cleaned repeatedly by acetone on one side, and their surfaces were roughened prior to spraying. The agglomerated powders were sprayed onto the substrates by ZB-2000 HVOF system (Beijing Zhen Bang Aerospace Precision Machinery Co. Ltd., Beijing, China). The samples produced by HVOF using the sub-micrometer, nanometer and the multimodal WC were denoted as B1, B2 and B3, respectively. Details of the optimized spraying parameters used to fabricate the coatings are illustrated in Table 2, and the thickness of the coatings was measured to be approximately 45 μm.

Table 2. Spray parameters employed during the HVOF spraying.

Parameters	Value
Spray distance, mm	240
Powder feed rate, g/min	12
Fuel (propane) pressure, MPa	0.6
Fuel gas (propane) flow rate, L/min	40
Oxygen pressure, MPa	0.8
Oxygen flow rate, L/min	220
Carrier gas nitrogen pressure, MPa	1.0
Carrier gas nitrogen flow rate, g/min	10
Gun traverse speed vertical plane, mm/s	60

2.3. Solar Absorbing Property and Coating Characterization

The solar absorbing and emitting properties of the deposited solar selective absorbing coatings were measured at room temperature. The near-normal spectral reflectance (R) and transmittance (T) of the coatings were measured in the wavelength range of 0.3~2.5 μm by a Shimadzu UV3600 UV/VIS spectrophotometer (Kyoto, Japan). The near-normal spectral reflectance in the wavelength range of 2.5~25 μm was measured by a Bruker Tensor 27 Fourier Transform spectrometer (Bruker, Karlsruhe, Germany). The absorptance (α) and emittance (ε) of the deposited coatings were calculated according to the reflectance by the following equations:

$$\alpha = \frac{\int_{0.3\mu m}^{2.5\mu m} I_{sol}(\lambda)(1 - R(\lambda))d\lambda}{\int_{0.3\mu m}^{2.5\mu m} I_{sol}(\lambda)d\lambda} \qquad (1)$$

$$\varepsilon = \frac{\int_{2.5\mu m}^{25\mu m} I_b(\lambda)(1 - R(\lambda))d\lambda}{\int_{0.3\mu m}^{2.5\mu m} I_b(\lambda)d\lambda} \qquad (2)$$

where $I_{sol}(\lambda)$ is the solar radiation power at AM1.5, $R(\lambda)$ is the spectral reflectance of the sample, and $I_b(\lambda)$ is the spectral black body emissive power at room temperature [18]. At least four samples were selected for spectral testing and the average values were used as the solar absorptance.

The phase compositions of the powders and coatings were analyzed by X-ray diffraction (XRD, D8 Advance, Bruker, Karlsruhe, Germany) employing Cu Kα radiation (λ = 1.54056 Å). The surface morphologies and chemical composition were characterized by scanning electron microscopy (SEM, JSM-IT300, JEOL Ltd., Tokyo, Japan), equipped with an energy dispersive spectrometer. The porosity measurements were performed by digital image analysis software SISC IAS V8.0 (Leica, Wetzlar, Germany).

3. Results

3.1. Phases Analysis

Figure 2 presents the X-ray diffraction patterns of the agglomerated powders and the sprayed coatings. It can be seen that only peaks of WC and Co phase are presented in the patterns of both the as-sprayed coatings and the agglomerated powders. This fact suggests that no decarburization occurred or the extent of decarburization, if any, was too small to be detected by the X-ray diffraction in the present experiment conditions. This can be ascribed to the fact that the agglomerated structure minimized the amount of feedstock powders that went through the high-temperature cycle due to the increment of momentum, thus limiting the amount of decarburization. Furthermore, the HVOF thermal spray gun is preferred over a plasma system due to the lower particle temperature and shorter residence time, which preserves a desirable WC phase and diminishes the tendency for decarburization.
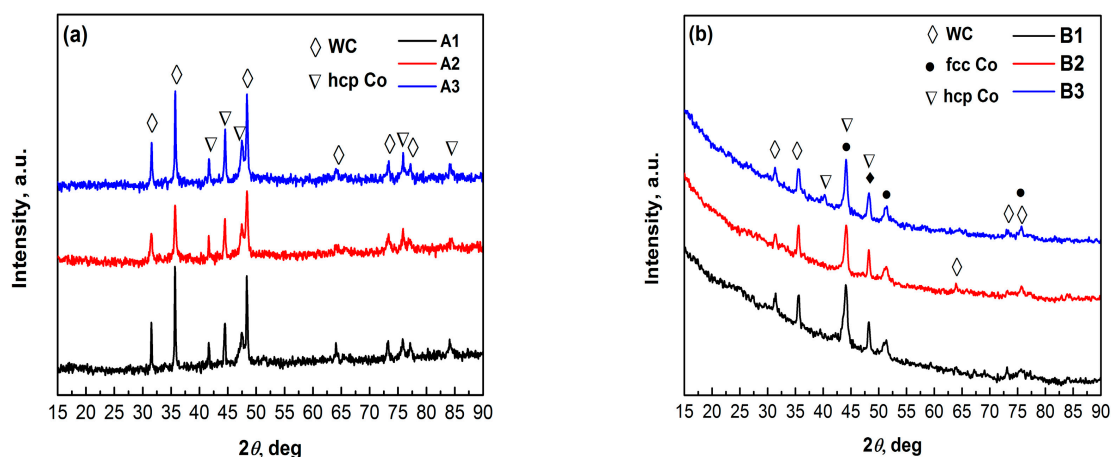

Figure 2. X-ray diffraction patterns of the agglomerated powders and the HVOF coatings: (**a**) the spray powders; (**b**) the HVOF coatings.

In addition, the X-ray powder diffraction patterns of the spray powders, as shown in Figure 2a, exhibit sharp and intense features, indicating their highly crystalline nature. Moreover, the Co phase in the spray powders exhibits a hexagonal structure as the three peaks appear at 41.7°, 44.2° and 47.6°, corresponding to (100), (002) and (101) of hcp-Co (ICSD 05-0727), respectively. However, the diffraction patterns of the sprayed coatings exhibit broaden peaks, indicating the presence of non-crystalline

phases. This can be attributed to the fact that the particles can reach quite high temperatures during the HVOF process, while they did not have enough time to crystallize under a high cooling rate [8]. Moreover, a portion of the Co phase was transformed into face-centered cubic structure by polymorphic transformation during the HVOF, as shown in Figure 2b, which would be beneficial to the adhesion strength to the substrate due to the good ductility of the face-centered cubic Co phase.

3.2. Solar Absorptance of the As-Deposited Coatings

Figure 3 shows the reflectance curves in 0.3–2.5 μm for the conventional and multimodal coatings together with the calculated absorptance. The multimodal absorbing coating (B3) exhibited a relatively high absorptance of 0.866, which was higher than the conventional coatings with values of 0.803 (B1) and 0.825 (B2), respectively. As the nano-sized WC can offer significant potential as a material showing enhanced or tunable light harnessing [19–22], thus the absorptance of sample B2 was measured to be higher than that of sample B1. The enhancement in solar absorptance in the multimodal (B3) coating over the conventional (B1 and B2) coatings will be discussed in Section 4.
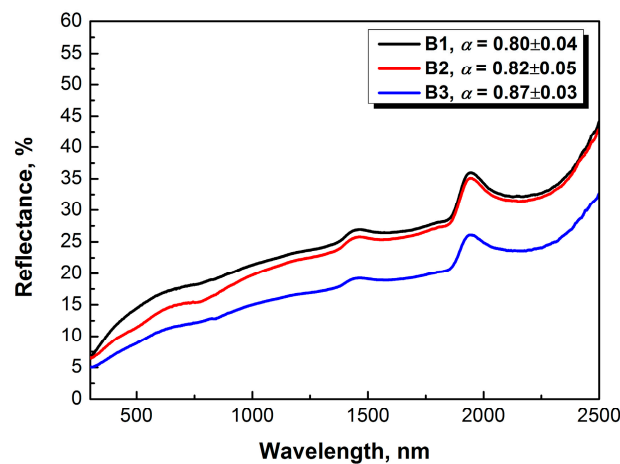

Figure 3. Reflectance spectra of the conventional (B1 and B2) and multimodal (B3) solar selective absorbing coatings deposited by HVOF.

4. Discussion

As shown above, the fabricated multimodal coating can combine the benefits of coarse and fine WC grains, leading to a better solar selectivity than what can be achieved by either fine or coarse grains alone. To better understand the enhancement in absorptance of the multimodal coating over the conventional coatings, the surface morphologies were examined, since the optical properties of the solar selective absorbing coatings are surface sensitive properties [23].

Figure 4 shows secondary electron SEM images of the HVOF deposited coatings. The as-deposited coatings consist of closely packed particles and micro-pores. Meanwhile some un-melted or semi-melted particles were also observed on the HVOF coatings. This is because the agglomerated particles resist being fully melted during the HVOF spraying process [24], and thus lead to a rather rougher surface for the HVOF coating (Figure 4b,d,f). The surface particles of the multimodal coating were finer than the conventional coatings, as shown in Figure 4a–c, which would increase the solar reflection and therefore be beneficial to the solar absorptance.
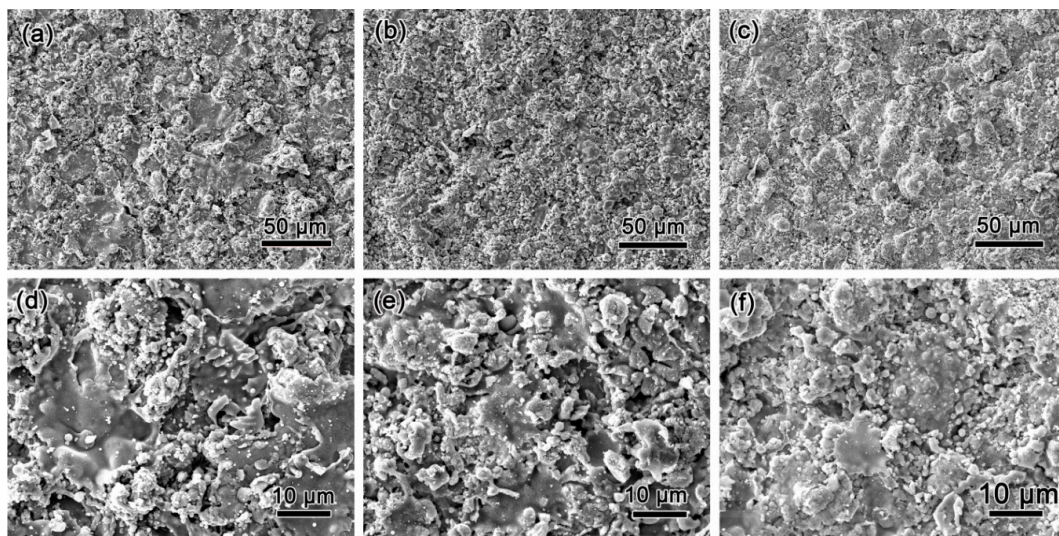
Figure 4. SEM micrographs of the conventional and multimodal coatings produced by HVOF: (**a**,**c**) sample B1; (**b**,**e**) sample B2; (**c**,**f**) sample B3.

Furthermore, the cross-section microstructures of the as-deposited coatings illustrated in Figure 5 shows pot-like WC grains varying in size from 1 to 3 μm and a Co-rich matrix. It has been established that the HVOF sprayed WC-Co coatings exhibit multi-phase microstructures with a lower fraction of WC than the starting agglomerated powders [25]. From these figures, it can be seen that all of the coatings bonded to the substrates well with no distinctive cracks. Moreover, the overall porosity percentages were estimated to be about 1% for the multimodal coating (B3), and 3% and 2% for the B1 and B2 coatings, respectively, which were lower than the reported values [26].
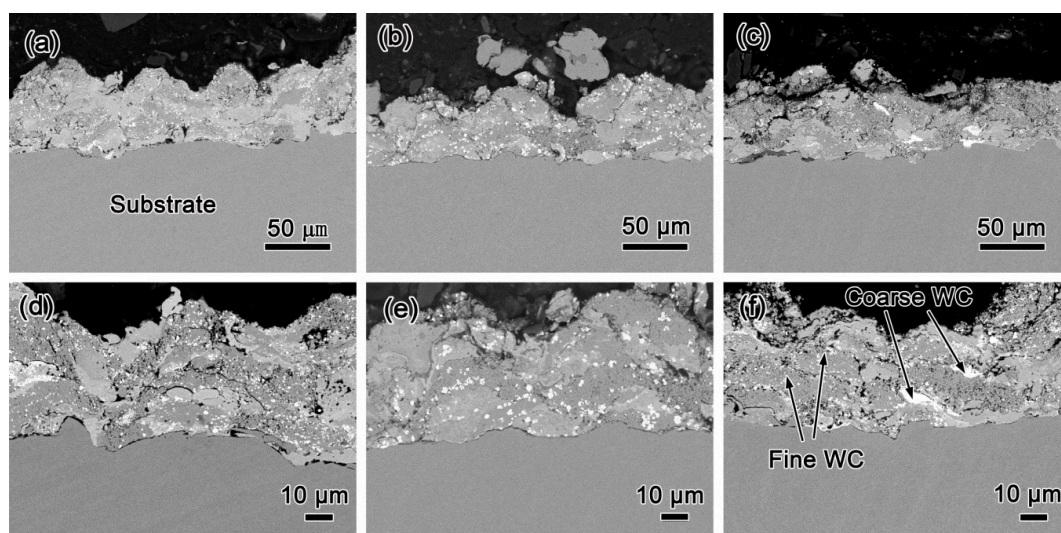

Figure 5. Backscattered SEM images from cross-sections of the coatings: (**a**,**d**) sample B1; (**b**,**e**) sample B2; (**c**,**f**) sample B3.

The formation of dense coatings by HVOF is closely related to the use of agglomerated feedstock. During the thermal spraying, particles of different sizes respond to the combustion flame differently. The nanostructured WC particles adhering to the surface underwent rapid melting due to the large surface area while leaving the coarse WC particles largely un-melted, but softened by heating. In this case, the heated but not necessarily melted part of the particle retains the original micro-porosity when

it impacts the substrate. The molten nano-WC would fill the available pores between the softened and heated aggregates, providing a dense spray-deposited coating. In addition, the large particle velocities and lower particle temperatures during HVOF can also contributed to further densification of the coating.

The WC grains would dissolve into the liquid metal, resulting in a solution of tungsten and carbon in cobalt. After the agglomerated powders reaching the substrate, the semisolid nanoparticles can provide a matrix in which the coarser particles remain embedded. The multimodal coating consists of coarse and fine WC grains, as shown by the arrows in Figure 5f, which is helpful for the formation of a denser coating than what can be accomplished by either coarse or fine grains alone.

It is worth noting that the element distributions in the multimodal coating and the conventional coatings are somewhat different, as shown in Figure 6. The gray regions were identified by energy dispersive spectrometer (EDS, JEOL, Ltd., Tokyo, Japan) analysis to be the Co-rich phase. Further examination suggested that the gray and bright regions contained dissolved W element and C element in addition to Co element. The bright regions were identified to contain higher levels of tungsten due to a greater degree of WC particle dissolution [25]. According to the EDS maps for carbon distribution, the multimodal coating (B3) has a lower content of bright phase, which suggests the agglomerated powders can prevent the dissolution of WC into the Co phase during spraying.
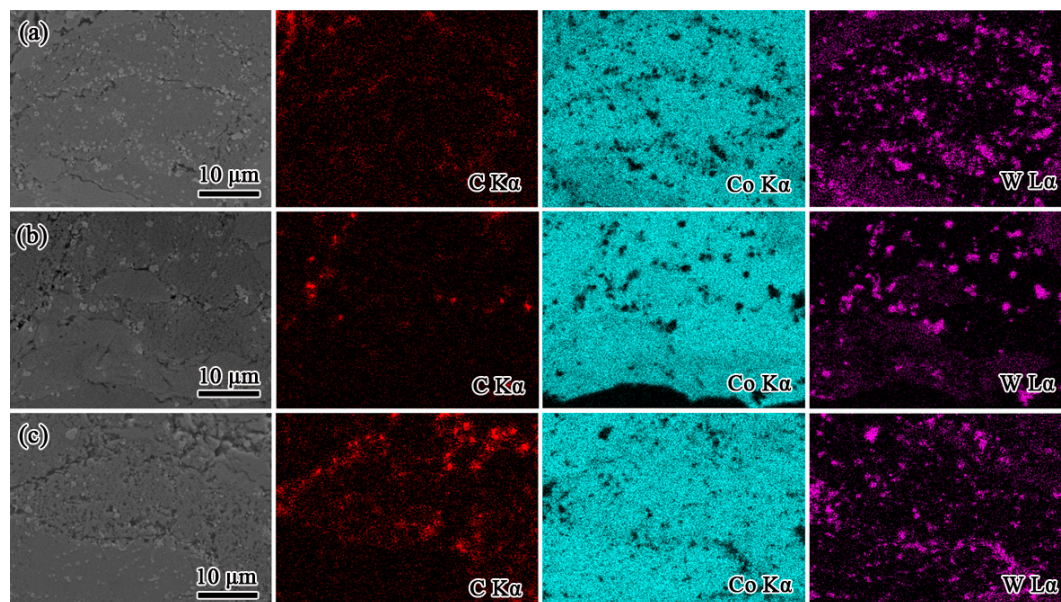

Figure 6. Backscattered SEM micrographs and EDS (energy dispersive spectrometer) analysis from cross-sections of the coatings: (**a**) sample B1; (**b**) sample B2; (**c**) sample B3.

In addition, the multimodal coating exhibited a more uniform element distributions combined with the coarse and fine WC particles, as illustrated in Figure 7. The formation of multimodal WC particles in the multimodal coating can be directly related to the following three factors: The formation of multimodal WC particles in the multimodal coating can be directly related to the melting behaviors of coarse and fine WC particles. The nanometer WC particles have lower softening and melting temperatures than the sub-micrometer WC particles, due to the larger surface area to volume ratio. Thus, the fine WC particles were sufficiently melted during HVOF and distributed uniformly among the grain boundaries of Co grains, while the coarse WC particles distributed unevenly due to their insufficient melting. In addition, the momentum of coarse WC particles was larger than that of fine WC particles. The coarse and fine WC particles cannot reach the substrate simultaneously, which would lead to a difference in deformation degree. Thus, the coarse WC particles exhibited a flat shape, as shown in Figure 5f.
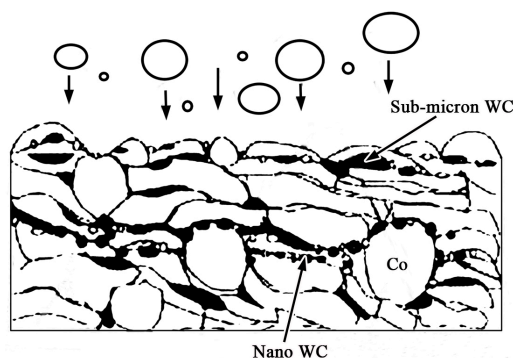
Figure 7. Sketch map of the formation of coarse and fine WC particles in the multimodal coating.

As described above, there is a benefit to solar absorptance by using a multimodal feedstock powder for thermal spraying. The enhancement in the solar absorptance results from a strong interaction with light in the multimodal coating consisting of coarse and fine WC particles. For nano-scaled WC particles, the interaction with light is significantly enhanced as the resonant absorption of solar by plasmons, which are collective oscillations of large concentrations of nearly free electrons [27]. Meanwhile, the multimodal distributed WC layer can enhance the solar reflection, which can further increase the solar absorptance.

Furthermore, the multimodal WC coating offered great potential for light-trapping, as the nano-WC showed enhanced or tunable light harnessing characteristics. Light was reflected between the sub-micrometer WC particles and the uniform nanometer WC particles, resulting in more efficient light-trapping properties in the multimodal WC coating than in the conventional coatings. However, further optimization of the coating, including particle size selection, particle distribution and coating surface morphology, is likely to increase the solar absorptance even more. Thus, optimal parameters, such as particle size range and distribution, warrant further investigation.

5. Conclusions

Multimodal WC/Co coating with coarse and fine WC particles fabricated by HVOF using agglomerated feedstock powders exhibited a higher solar absorptance than what can be achieved by either coarse or fine powders alone. The enhancement in solar absorptance of the multimodal WC/Co coating was attributed to the formation of a dense coating with no decarburized phases as well as the layer of distributed WC particles formed during the thermal spraying. These results indicate that the multimodal WC/Co absorbing coating fabricated by HVOF could potentially be employed on a large scale for solar photo-thermal conversion.

Author Contributions: Xiaobo Wang and Xudong Cheng conceived and designed the experiments; Taoyuan Ouyang, Xiaohua Duan, Chengzhu Ke, Xuemin Zhang, Jin Min and Weiyang Guo performed the experiments; Xiaobo Wang analyzed the data; Xiaobo Wang contributed materials/analysis tools; Xiaobo Wang wrote the paper.

Conflicts of Interest: The authors declare no conflict of interest.

References

1. De Villiers Lovelock, H.L. Powder/processing/structure relationships in WC-Co thermal spray coatings: A review of the published literature. *J. Therm. Spray Technol.* **1998**, *7*, 357–373. [CrossRef]
2. Moon, J.; Lu, D.; VanSaders, B.; Kim, T.K.; Kong, S.D.; Jin, S.; Chen, R.; Liu, Z. High performance multi-scaled nanostructured spectrally selective coating for concentrating solar power. *Nano Energy* **2014**, *8*, 238–246. [CrossRef]

3. Nuru, Z.Y.; Arendse, C.J.; Nemutudi, R.; Nemraoui, O.; Maaza, M. Pt-Al$_2$O$_3$ nanocoatings for high temperature concentrated solar thermal power applications. *Phys. B Condens. Matter* **2012**, *407*, 1634–1637. [CrossRef]

4. Céspedes, E.; Wirz, M.; Sánchez-García, J.A.; Alvarez-Fraga, L.; Escobar-Galindo, R.; Prieto, C. Novel Mo-Si$_3$N$_4$ based selective coating for high temperature concentrating solar power applications. *Sol. Energy Mater. Sol. Cells* **2014**, *122*, 217–225. [CrossRef]

5. Zhang, Q.-C. Optimizing analysis of W-AlN cermet solar absorbing coatings. *J. Phys. D Appl. Phys.* **2001**, *34*, 3113. [CrossRef]

6. Toor, F.; Guneratne, A.C.; Temchenko, M. Metal-dielectric frequency-selective surface for high performance solar window coatings. *SPIE Proc.* **2016**. [CrossRef]

7. Teixeira, V.; Sousa, E.; Costa, M.F.; Nunes, C.; Rosa, L.; Carvalho, M.J.; Collares-Pereira, M.; Roman, E.; Gago, J. Spectrally selective composite coatings of Cr-Cr$_2$O$_3$ and Mo-Al$_2$O$_3$ for solar energy applications. *Thin Solid Films* **2001**, *392*, 320–326. [CrossRef]

8. Dent, A.H.; Horlock, A.J.; McCartney, D.G.; Harris, S.J. Microstructure formation in high velocity oxy-fuel thermally sprayed Ni-Cr-Mo-B alloys. *Mater. Sci. Eng. A* **2000**, *283*, 242–250. [CrossRef]

9. Li, C.J.; Ohmori, A.; Harada, Y. Effect of powder structure on the structure of thermally sprayed WC-Co coatings. *J. Mater. Sci.* **1996**, *31*, 785–794. [CrossRef]

10. Ma, N.; Guo, L.; Cheng, Z.; Wu, H.; Ye, F.; Zhang, K. Improvement on mechanical properties and wear resistance of HVOF sprayed WC-12Co coatings by optimizing feedstock structure. *Appl. Surf. Sci.* **2014**, *320*, 364–371. [CrossRef]

11. Sánchez, E.; Bannier, E.; Salvador, M.D.; Bonache, V.; García, J.C.; Morgiel, J.; Grzonka, J. Microstructure and Wear Behavior of Conventional and Nanostructured Plasma-Sprayed WC-Co Coatings. *J. Therm. Spray Technol.* **2010**, *19*, 964–974. [CrossRef]

12. Pan, Y.; Li, D.Y.; Zhang, H. Enhancing the wear resistance of sintered WC-Co composite by adding pseudo-elastic TiNi constituent. *Wear* **2011**, *271*, 1916–1921. [CrossRef]

13. Juang, R.-C.; Yeh, Y.-C.; Chang, B.-H.; Chen, W.-C.; Chung, T.-W. Preparation of solar selective absorbing coatings by magnetron sputtering from a single stainless steel target. *Thin Solid Films* **2010**, *518*, 5501–5504. [CrossRef]

14. Qiao, Y.; Fischer, T.E.; Dent, A. The effects of fuel chemistry and feedstock powder structure on the mechanical and tribological properties of HVOF thermal-sprayed WC-Co coatings with very fine structures. *Surf. Coat. Technol.* **2003**, *172*, 24–41. [CrossRef]

15. Shipway, P.H.; McCartney, D.G.; Sudaprasert, T. Sliding wear behaviour of conventional and nanostructured HVOF sprayed WC-Co coatings. *Wear* **2005**, *259*, 820–827. [CrossRef]

16. Skandan, G.; Yao, R.; Sadangi, R.; Kear, B.H.; Qiao, Y.; Liu, L.; Fischer, T.E. Multimodal coatings: A new concept in thermal spraying. *J. Therm. Spray Technol.* **2000**, *9*, 329–331. [CrossRef]

17. Skandan, G.; Yao, R.; Kear, B.H.; Qiao, Y.; Liu, L.; Fischer, T.E. Multimodal powders: A new class of feedstock material for thermal spraying of hard coatings. *Scr. Mater.* **2001**, *44*, 1699–1702. [CrossRef]

18. Liu, H.D.; Wan, Q.; Xu, Y.R.; Luo, C.; Chen, Y.M.; Fu, D.J.; Ren, F.; Luo, G.; Cheng, X.D.; Hu, X.J.; et al. Long-term thermal stability of CrAlO-based solar selective absorbing coating in elevated temperature air. *Sol. Energy Mater. Sol. Cells* **2015**, *134*, 261–267. [CrossRef]

19. Trice, J.; Favazza, C.; Garcia, H.; Sureshkumar, R.; Kalyanaraman, R. Design and optimization of plasmonic-based metal-dielectric nanocomposite materials for energy applications. *Physics* **2010**. [CrossRef]

20. Schaadt, D.M.; Feng, B.; Yu, E.T. Enhanced semiconductor optical absorption via surface plasmon excitation in metal nanoparticles. *Appl. Phys. Lett.* **2005**, *86*, 063106. [CrossRef]

21. Pillai, S.; Catchpole, K.R.; Trupke, T.; Zhang, G.; Zhao, J.; Green, M.A. Enhanced emission from Si-based light-emitting diodes using surface plasmons. *Appl. Phys. Lett.* **2006**, *88*, 161102. [CrossRef]

22. Cole, J.R.; Halas, N.J. Optimized plasmonic nanoparticle distributions for solar spectrum harvesting. *Appl. Phys. Lett.* **2006**, *89*, 153120. [CrossRef]

23. Granqvist, C.G. Solar energy materials. *Appl. Phys. A* **1991**, *52*, 83–93. [CrossRef]

24. Yuan, F.H.; Chen, Z.X.; Huang, Z.W.; Wang, Z.G.; Zhu, S.J. Oxidation behavior of thermal barrier coatings with HVOF and detonation-sprayed NiCrAlY bondcoats. *Corros. Sci.* **2008**, *50*, 1608–1617. [CrossRef]

25. Stewart, D.A.; Shipway, P.H.; McCartney, D.G. Microstructural evolution in thermally sprayed WC-Co coatings: Comparison between nanocomposite and conventional starting powders. *Acta Mater.* **2000**, *48*, 1593–1604. [CrossRef]

26. Verdian, M.M.; Raeissi, K.; Salehi, M. Corrosion performance of HVOF and APS thermally sprayed NiTi intermetallic coatings in 3.5% NaCl solution. *Corros. Sci.* **2010**, *52*, 1052–1059. [CrossRef]

27. Kittel, C. *Introduction to Solid State Physics*, 8th ed.; John Wiley and Sons, Ltd.: New York, NY, USA, 2005.